ABOVEGROUND BIOMASS ESTIMATION OF CAOHAI WETLAND VEGETATION BASED ON OPTICAL AND RADAR REMOTE SENSING

Z.H. WANG[1]*, H.Y. DAI[2], J.B. LIU[3], J.T. REN[4]

The aboveground biomass (AGB) of wetland vegetation is an important characterization of the structure and function of wetland ecosystems. Taking Caohai National Nature Reserve (CNNR) as the research object, three polarization combinations of two backscattering coefficients and 10 vegetation indexes were extracted from the GF-3 and Sentinel-2A, and the correlation between them and biomass were analyzed. Then, the AGB estimation models based on the integration of optical image and radar image were constructed. Based on the above research, the integration of optical and radar remote sensing was able to obtain the complete spatial distribution of biomass in the study area; which serves as a good reference value for the estimation of grassland AGB in cloudy and rainy areas.

Keywords: GF-3, Sentinel-2A, aboveground biomass, BP neural network

1. Introduction

The continuous development of remote sensing technology has led to great progress in research on remote sensing inversion of the aboveground biomass (AGB) of wetland vegetation. Many scholars have studied the use of NDVI, EVI, and other vegetation indexes to estimate the AGB of grassland based on the light energy utilization model [1,2], and satisfactory results have been achieved, but the model is complex, and its application is restricted to some extent [3]. The statistical model between the backscattering coefficient of synthetic aperture radar (SAR) image and vegetation biomass is simple and easy to implement, and its ability of penetrating cloud and fog has advantages in cloudy and rainy areas, but the disadvantages are lack of model parameters, low accuracy, and poor guarantee [4]. The spectral vegetation indexes can indirectly reflect vegetation coverage and biomass, so a linear or nonlinear relationship between wetland vegetation biomass

[1] PhD, College of Geoscience and Surveying Engineering, China University of Mining & Technology (Beijing), China, e-mail: jxbj457@126.com;
[2] Prof., College of Geoscience and Surveying Engineering, China University of Mining & Technology (Beijing), China, e-mail: dhy@cumtb.edu.cn;
[3] A.P., School of mining engineering, Guizhou University of Engineering Science, China, e-mail: liujibo@gues.edu.cn
[4] A.P., Guizhou Province Key Laboratory of Ecological Protection and Restoration of Typical Plateau Wetlands, China, e-mail: jintongabc@163.com;

and vegetation index can be established [4]. In order to get the best inversion accuracy, many scholars have studied and analyzed the selection of vegetation indexes [5,6]. In recent years, some indexes and red-edge indexes related to vegetation physical and chemical parameters, such as red-edge chlorophyll index (CI_{re}) and green chlorophyll index (CI_{green}), have been proven to be closely related to chlorophyll content [7-9]. Therefore, the red-edge bands should also have the potential to estimate the AGB of wetlands [10]. Sentinel-2A and Sentinel-2B satellites provide high spatial and temporal resolution multispectral data, and three red-edge bands were set up to provide more optional information for vegetation monitoring [8]. Some scholars' research shows that Sentinel-2 red-edge bands are of important value in estimating vegetation biomass [10,11].

Compared with the single linear regression of the empirical model method, the multiple regression model and back propagation neural network (BPNN) model based on optimal vegetation indexes have higher accuracy in the estimation of vegetation physical and chemical parameters [12,13]. The BPNN model is also commonly used in recent years, and the research of many scholars shows that it performs well in biomass estimation [12,14].

With the promotion of the ecological environment protection and comprehensive treatment project in CNNR, the wetland habitat has been significantly recovered and improved. Due to the perennial cloudy and rainy weather in Southwest China, optical images can be easily affected, so the integration of an optical image and a radar image for biomass estimation can give full access to the advantages of different remote sensing data [4]. Based on the above considerations, we first extracted 10 vegetation indexes (NDVI, EVI, SR, MERIS Terrestrial Chlorophyll Index (MTCI), MSR, MSR_{re}, $NDVI_{re}$, SR_{re}, CI_{re}, and CI_{green}) from multispectral Sentinel-2A data. Then, the indexes with high correlation with biomass were selected as the independent variables to construct the estimation model. For the cloud covered area, based on the dual polarimetric SAR data of GF-3, the different combinations of backscattering coefficients (HH/HV, (HH+HV)/(HV−HH), and HH−HV) were calculated, then the BPNN model was constructed to estimate the biomass.

2. Research Area and Data Acquisition

2.1 Research Area Overview

CNNR, a subtropical plateau wetland ecosystem, is listed as a nationally important wetland [18]. Its special location and natural environment provides habitat for rare birds and migratory birds. The reserve is located in the central part of the Yunnan–Guizhou Plateau and in the hinterland of Wumeng Mountain. Caohai lake belongs to the Yangtze River system and is the upper source lake of the Hengjiang River, which is a tributary of the Jinsha River [15]. The scope of

this study centered on the protected area (center latitude and longitude are 1105°18′27″ and 27°17′50″, respectively), and focused on the AGB of the water buffer zone and grassland in the catchment areas such as Huyelin, Bojiwan, and Zhujiawan. The range and distribution of samples of the nature reserve are shown in Figure 1, whose base map is the Sentinel-2A image taken on July 21, 2018.

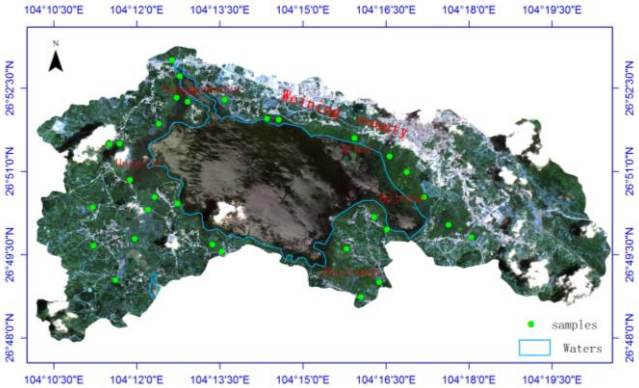

Fig. 1. Reserve and distribution of sampling points

2.2 Field Data Measurement

The vegetation growth on the Guizhou plateau reaches its peak in early August, and then begins to decline [16]. There were 31 survey points, mainly distributed in the catchment area and water outlet and other areas with complete grassland and little human impact. The data collected included grassland biomass and typical vegetation spectra. The sampling method of biomass was to select a 10 m × 10-m area, then five 0.5 m × 0.5-m sample points in the four corners and center of the area were selected to collect the aboveground part of vegetation. At last, the collected vegetation was dried to a constant weight using a dryer in the laboratory. Then, the AGB dry weight ($g \cdot m^{-2}$) of dried vegetables was calculated as measured values [4][10]. The optical image used was from Sentinel-2A on July 21, 2018, and the radar data was from GF-3 on July 15, 2018. The sampling dates are July 26 and July 27, both with cloudy and sunny weather.

2.3 Satellite Data and Data preprocessing

The Gaofen-3 satellite (GF-3) is a remote sensing satellite of China's Gaofen special project. GF-3 is the C-band synthetic aperture radar data, with 12 modes such as SL, UFS, FS and QPS. This study used FS Ⅱ dual-polarization SAR data with a resolution of 10×(8～12) m, which consists of HH and HV polarization channels. Sentinel-2A multispectral data include 13 bands, of which the visible and near-infrared bands have the highest resolution (10 m). The ESA SciHub publishes L1C-level data that provide a geometrically corrected orthophoto without radiometric calibration and atmospheric correction.

The pretreatment steps of GF-3 dual polarimetric SAR include multi-look processing, filtering and noise reduction, radiometric calibration, and geocoding. Sentinel-2A L1C data are derived from atmospheric apparent reflectance, which needs radiometric calibration and atmospheric correction to obtain surface reflectance data. For this reason, we used the sen2cor tool of the ESA to process L1C data into L2A data. Finally, the resulting data of each band were resampled to 10 m.

3. Research Methods

3.1. Estimation Parameter Selection

The spectral vegetation index method is an effective method for remote sensing inversion of vegetation parameters. In this study, 10 vegetation indexes (Table 1) were selected to explore the relationship between vegetation indexes and grassland biomass based on Sentinel-2A multispectral image data. The correlation between reflectance and chlorophyll content at 705 nm is better than that of other red-edge bands [11,12]. Therefore, the 705-nm vegetation red-edge of Sentinel-2A was used as the red-edge band in the calculation formula.

Research shows that different polarization combinations of the radar can weaken the impacts of noise on the backscattering coefficient of ground objects [17] and can reflect the characteristics of ground objects from more angles and broaden the information scope of ground objects [18]. According to past research publications and preliminary experiments, three types of backscattering coefficient polarization combinations, namely HH/HV, (HH+HV)/(HV−HH), and HH−HV, were selected.

Table 1

Vegetable indexes and polarization combination modes selected in this study

Estimation Parameters	Formulas	Reference Sources
Normalized Difference Vegetation Index(NDVI)	$(R_{nir} - R_{red}) / (R_{nir} + R_{red})$	(Schell etc.,1973)[18]
Enhanced Vegetation Index(EVI)	$2.5(R_{nir} - R_{red}) / (R_{nir} + 6R_{red} - 7.5R_{blue} + 1)$	(Huete etc.,2002) [19]
Simple Ratio(SR)	R_{nir} / R_{red}	(Jordan etc.,1969) [20]
MERIS Terrestrial Chlorophyll Index(MTCI)	$(R_{nir} - R_{red-edge}) / (R_{red-edge} - R_{red})$	(Dash and Curran,2004)[21]
Modified Simple Ratio(MSR)	$(R_{nir} / R_{red} - 1) / \sqrt{R_{nir} / R_{red} + 1}$	(Chen etc.,1996)[22]
Modified red-edge Simple Ratio(MSRre)	$(R_{nir} / R_{red-edge} - 1) / \sqrt{R_{nir} / R_{red-edge} + 1}$	(Wu etc.,2008)[23]
Red-edge NDVI(NDVIre)	$(R_{nir} - R_{red-edge}) / (R_{nir} + R_{red-edge})$	(Sims and Gamon,2002)[24]
Red-edge Simple	$R_{nir} / R_{red-edge}$	(Sims and

Ratio(SRre)		Gamon,2002)[24]
red-edge chlorophyll index(CIre)	$R_{nir} / R_{red-edge} - 1$	(Gitelson etc.,2005)[7]
Green Chlorophyll Index(CIgreen)	$R_{nir} / R_{green} - 1$	(Gitelson etc.,2005)[7]
HH/HV	HH/HV	/
HH-HV	HH-HV	/
(HH+HV)/(HV-HH)	(HH+HV)/(HV-HH)	/

Note: HH and HV are the corresponding radar backscatter coefficients.

3. 2. Biomass Estimation and Evaluation

With the curve fitting tool in MATLAB, the indexes in Table 1 were optimally fitted with AGB. The root mean square error (RMSE) and the coefficient of determination (R^2) were used to evaluate the accuracy of the fitted results of biomass and different indexes. Finally, the vegetation indexes with high correlation were selected to construct the multiple nonlinear regression model and BPNN model for biomass estimation.

3. 2.1. Multiple Regression Model and BPNN model

The approach of the multiple nonlinear regression model is to construct the research object into multiple functions and determine the parameters of each function [25]. Based on the analysis of the correlation between vegetation indexes and biomass, the indexes with better correlation and their fitting functions of biomass were selected, and then the multivariate nonlinear biomass estimation model was constructed based on the principle of linear superposition. The expression of the AGB multiple nonlinear regression model is as follows:

$$AGB = a_1 e^{b_1 x_1} + a_2 x_2 + a_3 e^{b_3 x_3} + c \quad (1)$$

In the formula, a_1, a_2, a_3, b_1, b_3 and c are parameters to be determined, x_1, x_2 and x_3 correspond to the indexes with high correlation with biomass.

BPNN is composed of an input layer, hidden layer, and output layer. Its core idea is to use gradient descent method to solve the minimum value of the objective function with the square of network error [25]. It is generally believed that three-layer BPNN can approximate any continuous function [14]. Based on the MATLAB R2018a programming environment, the specific processes are as follows:

(1) The sample values are linearly normalized with the following formula to ensure that the values are within (0,1).

$$\hat{x} = a + b\frac{p - x_{\min}}{x_{\max} - x_{\min}} \quad (2)$$

In the formula, $\hat{x}$ is the normalized values, and *a* and *b* are the parameter values for normalization, which can be adjusted appropriately during processing.

P is the value to be normalized, $x_{\max}$ is the maximum value in the sequence value, and $x_{\min}$ is the minimum value.

(2) Input the training eigenvectors $\{X_i\}$ and the target vectors $\{Y_i\}$ into BPNN, X_i is the index eigenvector of sample *i*, Y_i is the biomass of sample *i*.

(3) In the hidden layer, the actual output value y_j of each node neuron is calculated according to Equations (3) and (4) to complete a forward propagation.

$$y_i = f(\sum_{j=0}^{k} W_{ij} x_i) \quad (j=1,2,\ldots,k) \tag{3}$$

$$f(x) = \frac{1}{1-e^{-(x-\theta)}} \tag{4}$$

Here, W_{ij} is the weight of the *j*th neuron in the *i*th layer of the hidden layer, θ is the threshold, and *f(x)* is the transfer function sigmoid.

(4) The errors between target output *Y* and target $\hat{y}$ of the network system is defined as E_i, and its formula is as follows:

$$E_i = \frac{1}{2}\sum (y_i - \hat{y}_i)^2 \tag{5}$$

(5) The partial derivative of E_i to *W* is used to represent the gradient direction of the weights. Back propagation based on formula (6) is then used to adjust the weights of each node neuron in each hidden layer.

$$W(t+1) = W\ (t) + \eta(-\partial E / \partial W)\,|_{W=W(t)} \tag{6}$$

Here, η is the learning rate.

3.2.2. Evaluation methods

The SPSS Statistics 24.0 software was used for random sampling of 31 measured biomass values, and 16 were selected as modeling samples and 15 as test samples. The accuracy of the models were evaluated based on the relative mean error (RME) and mean absolute error (MAE). The formulas used are:

$$MAE = \frac{1}{N}\sum_{i=1}^{N} |y_i - y_i'| \tag{7}$$

$$RME = \frac{\sqrt{1/N\sum_{i=1}^{N}(y_i - y_i')^2}}{y} \times 100\% \tag{8}$$

Here, y_i is the measured hay weight, y_i' is the estimated hay weight, and y is the average hay weight measured in samples. All measurement units of them are g/m^2, and N is the number of sampling points.

4. Results Analysis and Discussion

4.1. Correlation Analysis

Figure 2 shows the scattered point-fitting curve between indexes and biomass, with R^2 greater than 0.60. It can be seen from Figure 2 that SR_{re} (R^2 = 0.88, RMSE = 110.2 g·m^{-2}) performed the best. For the fitting performance between the radar backscattering coefficient and biomass, ranked by R^2 from highest to lowest: (HH+HV)/(HV−HH) > HH/HV = HH−HV. Compared to the red-edge indexes of SR_{re}, MSR_{re}, and $NDVI_{re}$, along with the common indexes of SR, MSR, and NDVI, it can be seen that the red-edge indexes increased the accuracy of biomass estimation to different degrees.

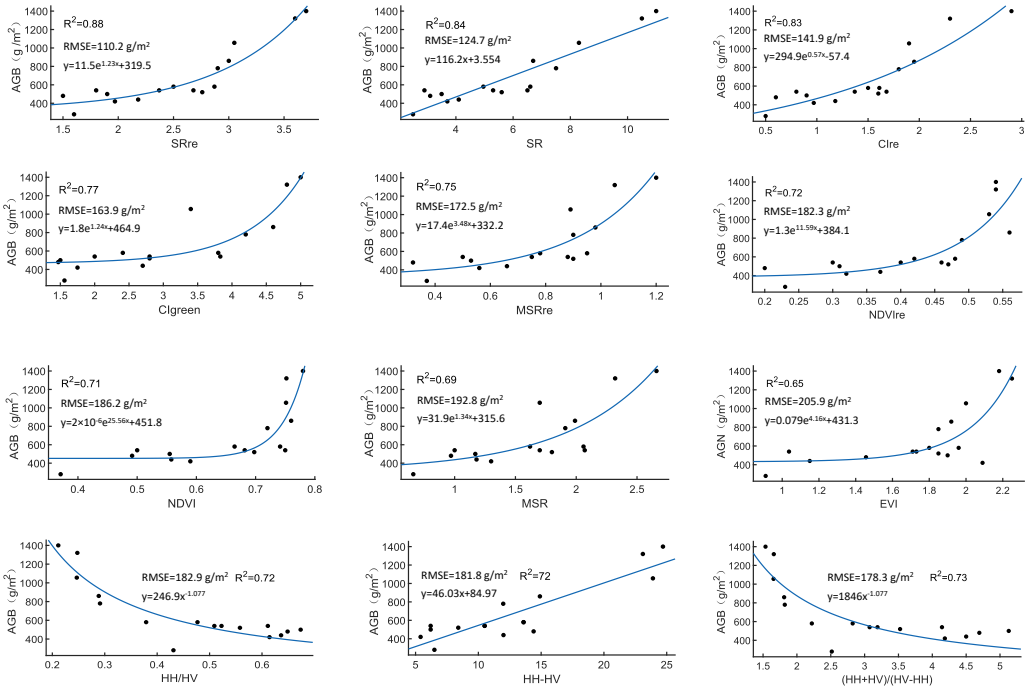

Fig. 2. Relationships between AGB and vegetation indexes

It was necessary to perform an accuracy test on the simulation results. The number of check samples was 15 and the RME was used to test the accuracy of this model. The errors, listed in ascending order, are as follows: SR_{re} (13.5%) > SR (15.3%) > CI_{re} (17.4%) > CI_{green} (20.1%) > MSR_{re} (21.2%) > (HH+HV)/(HV−HH) (22.1%) > $NDVI_{re}$ (22.4%) > NDVI (22.9%) > HH/HV(23.9%) > HH−HV (25.3%). The SR_{re} had the smallest error, and the HH−HV error was the largest, which was consistent with the accuracy order of the models. The HH/HV, HH−HV, and (HH+HV)/(HV−HH) were significantly correlated at 0.05 level.

4.2. Biomass estimation based on multiple nonlinear regression

Three indexes (SR_{re}, SR, and CI_{re}) with R^2 greater than 0.8 were selected to construct the multivariate functional relationship between AGB and VIs. Sixteen groups of samples were used to calculate the model parameters, and lstOpt's "Levenberg Marquardt method + general global optimization method" was used to solve the parameters in model (1), and then the multiple nonlinear regression model expression of AGB was obtained as follows:

$$AGB = 7.67e^{1.34x_1} - 2.13x_2 - 4997.01e^{-8.09x_3} + 372.39 \quad (9)$$

The fitting accuracy R^2 and RMSE of model (9) were 0.9 and 96.85 $g \cdot m^{-2}$, respectively. It can be seen from Figure 3 that the change trend of AGB predicted value of model (9) was consistent with the measured value, which was close to the 1:1 line, and the determination coefficient R^2 was 0.89. The mean absolute error (MAE) and mean relative error (RME) were used to evaluate the accuracy of the model. The MAE of the multivariate nonlinear model was 89.40 $g \cdot m^{-2}$, and the RME was 12.2%. The MAE of the multivariate linear model was 121.52 $g \cdot m^{-2}$, and the RME was 18.1%.

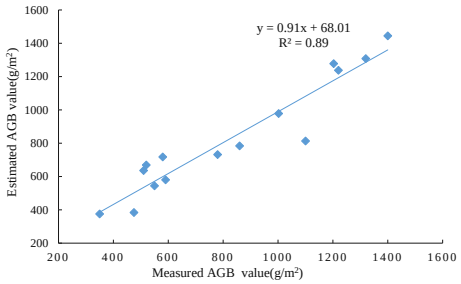

Fig.3. Fitting effect of prediction model

4.3. Biomass estimation based on BPNN

A standard BPNN was established, where the hidden layer used the tansig activation function, the output layer used the sigmoid activation function, and the dynamic gradient function was used to train the samples. The weight and displacement of the hidden layer were set between rands (−1,1). The optimal parameters were judged by the minimum mean square error between the predicted output values and the sample values for verification. In order to improve the convergence speed and prediction accuracy of the network, the sample values were normalized by equation (2), parameter a was set to 0.1, parameter b was set to 0.8, and the sample values were normalized to (0,1). The Levenberg–Marquardt (LM) algorithm was used to train the sample values. This method not only retained the local convergence, but also had the global property of gradient descent method, with fast convergence and fewer iterations so as to improve

BPNN. The BPNN was constructed by using three vegetation indexes with R^2 greater than 0.8 as input variables in Figure 2. The number of nodes in the hidden layer was determined as 10, learning rate was 0.05, the maximum training times were 10,000, and the target accuracy was 0.00001. Similarly, for SAR data, the input variables of BPNN were HH/HV, HH−HV, and (HH+HV)/(HV−HH).

The R^2, MAE, and RME between testing samples and biomass predicted by BPNN based on optical vegetation indexes were 0.93, 75.46 g·m^{-2}, and 10.2%, respectively. The R^2, MAE, and RME between testing samples and biomass predicted by BPNN based on SAR were 0.8, 129.26 g·m^{-2}, and 18.6%, respectively.

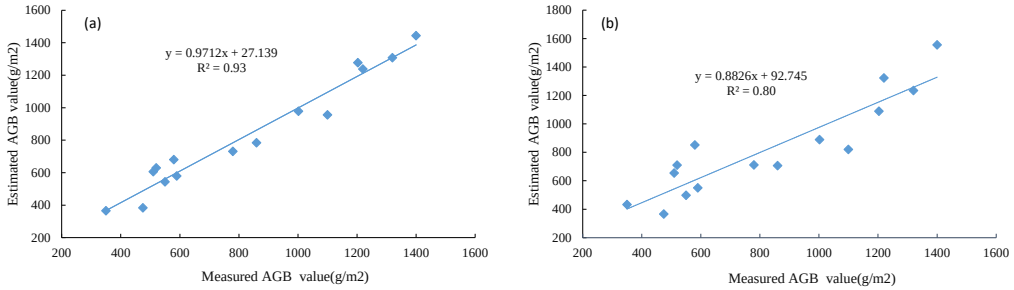

Fig.4. Prediction effect of optical index (a) and SAR (b) based on BPNN model

4.4. Spatial Distribution of Biomass

The image data of the three polarization combinations were preprocessed and put into the BPNN model to obtain the biomass estimation results. In order to remove the influence of noise on biomass mapping, the biomass of grassland and cultivated land was extracted for mapping (as shown in Figure 5).

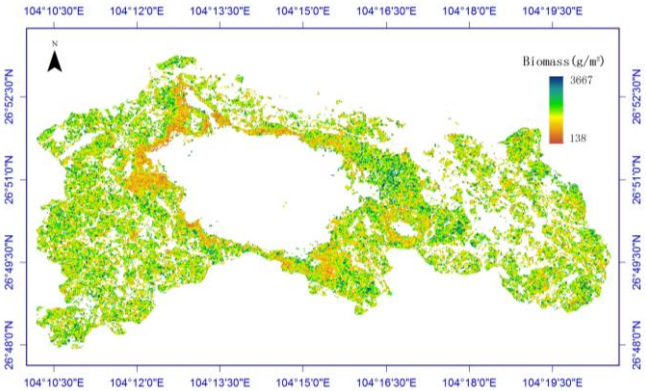

Fig.5. Aboveground biomass distribution inversed by the radar model

Similarly, after preprocessing the SR_{re}, SR, and CI_{re} images, the biomass estimation results were obtained by the BPNN model. For the cloud-covered parts of Sentinel-2A optical image, the biomass retrieved from SAR was used to

supplement the missing parts to obtain the biomass distribution map of the whole region, as shown in Figure 6.

The areas with biomass value lower than 250 $g \cdot m^{-2}$ were mainly non-vegetated areas such as construction land, water area, and unused land, which had no practical significance and were removed during mapping. In the northeast of Caohai Lake, the grassland from Xihai to Bojiwan was the most lush, with a large number of verdant plants such as *Acorus calamus*, *Phragmites australis*, and *Alternanthera philoxeroides*. Its biomass was the highest, generally more than 1,000 $g \cdot m^{-2}$. In addition to the grassland type, the reason was also related to the inflow of some eutrophic urban wastewater in northeast Caohai. The biomass of corn planting areas was also relatively high.

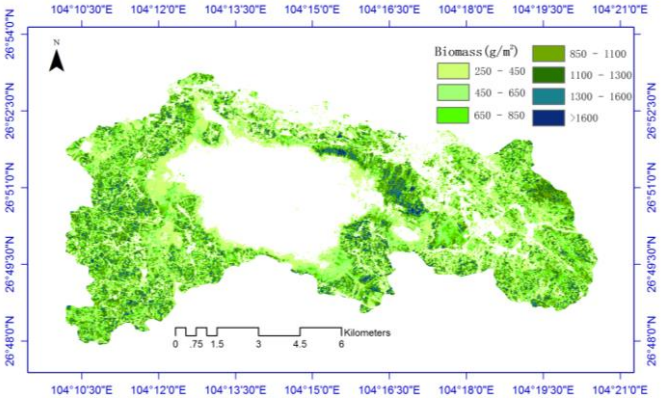

Fig.6. Biomass distribution of the Caohai Reserve

The catchment basins of Huyelin, Bojiwan, Xihai, Zhujiawan, Wujiayantou, and Yangguanshan were important foraging and habitats of the black-necked crane and other rare and migratory birds; there were numerous hygrophytes (excluding submerged and floating plants), and their vegetation growth was of great significance to measure ecological changes. In the shallow water area of Yangguanshan, the biomass of the hygrophytes ranged from 400 $g \cdot m^{-2}$ to 600 $g \cdot m^{-2}$, and they were mainly sedge, cordyceps, and some stretches of *Phragmites australis*. In the shallow water area of Huyelin, the hygrophytes were mainly spartina and bermudagrass, while in the offshore area, it was *Phragmites australis*, with biomass ranging from 400 to 850 $g \cdot m^{-2}$. Zhujiawan was 2.5-km long and 1.2-km wide; nearly half of the area was planted with crops, mainly corn and some vegetables, and the rest were hygrophytes; the biomass ranged from 400 to 800 $g \cdot m^{-2}$. During the period of field investigation, the corn in the corn planting area was going through silking to filling, and the biomass was between 800 and 1600 $g \cdot m^{-2}$. Bojiwan was connected with the West Sea; it had a large area of hygrophytes, as well as some grassland and vegetable crops. There were many kinds of vegetation such as bermudagrass, *Phragmites australis*, *Acorus calamus*,

Alternanthera philoxeroides, and *Polygonum hydropiper*. It was the most prosperous area around the lake. There was a large reed area in Jiangjiawan with a biomass of about 1,100 $g \cdot m^{-2}$. The total biomass calculated in this paper was about 360 kilotons and the annual average NPP of MODIS NPP from 2007 to 2015 was about 500 kilotons.

5. Conclusions

(1) The three polarization combinations of backscattering coefficient extracted from Sentinel-1A had significant correlations with biomass ($0.72 \leq R^2 \leq 0.73$, $178.3\ g \cdot m^{-2} \leq RMSE \leq 182.9\ g \cdot m^{-2}$).

(2) The vegetation indexes calculated by Sentinel-2A were significantly correlated with AGB of wetland vegetation ($0.55 \leq R^2 \leq 0.88$, $110.2\ g \cdot m^{-2} \leq RMSE \leq 216\ g \cdot m^{-2}$). Of them, SR_{re} had the highest correlation ($R^2 = 0.88$, $RMSE = 110.2\ g \cdot m^{-2}$), followed by SR and CI_{re}; the correlation between vegetation indexes (SR_{re}, $NDVI_{re}$, MSR_{re}) and biomass were improved by adding red-edge bands.

(3) SR_{re}, SR, and CI_{re} with R^2 values greater than 0.8 were selected to construct the multivariate nonlinear regression model and BPNN model. The results showed that the BPNN model was the best model, and the MAE and RME of the simulated values tested by test data were 75.46 $g \cdot m^{-2}$and 10.2%, respectively. Based on the BPNN model constructed by three polarization combinations of backscattering coefficient, R^2, MAE, and RME tested by test data were 0.79, 130.27 $g \cdot m^{-2}$, and 18.5%, respectively.

(4) In the cloudy and rainy Guizhou province, it was possible that the BPNN model based on vegetation indexes and the polarization combinations of the model were integrated to retrieve vegetation biomass, which compensated for the limitation that optical images could not obtain biomass in a cloudy area.

Acknowledgments

We thank LetPub (www.letpub.com) for its linguistic assistance during the preparation of this manuscript.

R E F E R E N C E S

[1]. *X.L. Ren, H.L. He, L. Zhang, et al*, Research of Environmental Sciences, **vol. 30**, no. 1, 2017, pp. 51-58, 2017

[2]. *L.Y. Zhang, G. Wang, L.R. Bao, et al*, Pratacultural Science, **vol. 25**, no. 3,2008, pp.6-11

[3]. *W.Q. Zhu, Y.H. Chen, D. Xu, et al*, Chinese Journal of Ecology, **vol. 24**, no. 03,2005, pp. 296~300

[4]. *P. Wang, R.R. Wan, G.S. Yang*, Wetland Science, **vol. 15**, no. 01,2017, pp.114-124

[5]. *G.Q. Yang, Y. Ma, J.B. Wang, et al*, Marine Environmental Science, **vol. 37**, no. 01,2018, pp.78-85+94

[6]. *Kross A, Mcnairn H, Lapen D, et al,* International Journal of Applied Earth Observations & Geoinformation, **vol. 34**, no. 1,2015, pp.235-248
[7]. *Gitelson A A, Viña A, Ciganda V, et al*, Geophysical Research Letters, **vol. 32**, no. 8,2005,93-114
[8]. *Y. Tian, Z.Q. Chen, F.M. Hui, et al*, Journal of Beijing Normal University (Natural Science), **vol. 55**, no. 01,2019, pp.57-65
[9]. *W. Su, X.F. Zhao, Z.P. Sun, et al*, Spectroscopy and Spectral Analysis, **vol. 39**, no. 05,2019, pp. 1535-1542
[10]. *Y. Zheng, B.F. Wu, M. Zhang,* Journal of Remote Sensing, **vol. 21**, no. 2,2017, pp.318-328
[11]. *Shoko C, Mutanga O, Dube T,* Remote Sens.10, 564, 2018.
[12]. *Tang, Chen, Jiang,* J APPL SPECTROSC+, **vol. 84**, no. 4,2018, pp.627-632.
[13]. *W. Xiao, J.L. Chen, H.Z. Da, et al*, Transactions of the Chinese Society for Agricultural Machinery, **vol. 49**, no. 08,2018, pp.169-180
[14]. *H. Xu, P. Pang, J.K. Ning, et al*, Journal of Northeast Forestry Univetsity, **vol. 46**, no. 01,2018, pp.63-67
[15]. *J.T. Ren, S.J. Mo, Q.L. Chen, et al*, Journal of Xinyang Normal University (Natural Science Edition), (03),2017, pp. 385-392
[16]. *Y.F. Zheng, H.J. Liu, R.J. Wu, et al*, Journal of Ecology and Rural Environment, **vol. 25**, no. 01,2009, pp.12-17
[17]. *C. Ma,* Transactions of the Chinese Society of Agricultural Engineering (Transactions of the CSAE), **vol.34**, no. 2,2018, pp.153－158
[18]. *Schell J A*, Nasa Special Publication, 1973, pp.351-309
[19]. *Huete A, Didan K, Miura T, et al*, Remote Sensing of Environment, **vol. 83**, no. 1,2002, pp.195-213
[20]. *Jordan C F*, Ecology, **vol. 50**, no. 4,1969, pp.663-666
[21]. *Dash J, Curran P J*, International Journal of Remote Sensing, **vol. 25**, no. 23,2004, pp.5403-5413
[22]. *J.M. Chen*, Canadian Journal of Remote Sensing, **vol. 22**, no. 3,1996, pp.229-242
[23]. *C. Wu, N. Zheng, T. Quan, et al*, Agricultural & Forest Meteorology, **vol. 148**, no. 8,2008, pp.1230-1241
[24]. *Sims D A, Gamon J A*, Remote Sensing of Environment, **vol. 81**, no. 2, 2002, pp.337-354
[25]. *Huang J, Jing PW, Li M,* Transactions of the Chinese Society for Agricultural Machinery, **vol. 47**, no. 08,2016, pp.171-178